INTERNATIONAL JOURNAL FOR NUMERICAL METHODS IN FLUIDS, VOL. 9, 167–183 (1989)

NUMERICAL SIMULATION OF AXISYMMETRIC TURBULENT FLOW IN COMBUSTORS AND DIFFUSERS

CHAIN-NAN YUNG,* THEO. G. KEITH, JR.† AND KENNETH. J. DE WITT*

Department of Chemical Engineering and Department of Mechanical Engineering,† University of Toledo, Toledo, Ohio, U.S.A.*

SUMMARY

Numerical studies of turbulent flow in an axisymmetric 45° expansion combustor and bifurcated diffuser are presented. The Navier–Stokes equations incorporating a k–ε model were solved in a non-orthogonal curvillinear co-ordinate system. A zonal grid method, wherein the flow field was divided into several subsections, was developed. This approach permitted different computational schemes to be used in the various zones. In addition, grid generation was made a more simple task. However, treatment of the zonal boundaries required special handling. Boundary overlap and interpolating techniques were used and an adjustment of the flow variables was required to assure conservation of mass flux. Three finite differencing methods—hybrid, quadratic upwind and skew upwind—were used to represent the convection terms. Results were compared with existing experimental data. In general, good agreement between predicted and measured values was obtained.

KEY WORDS Axisymmetric turbulent flow Combustors Diffusers Navier–Stokes equations k–ε model Zonal grid Finite differences

INTRODUCTION

Over the past several years, numerical computation of turbulent flows has been an active research subject. Because of the complexity involved in finding solutions, most turbulent flow studies have dealt with flows in regularly shaped geometries in which the boundaries coincided with the co-ordinate lines of either a Cartesian or a cylindrical co-ordinate system. For irregularly shaped flow domains, in which the mesh points of the grid system do not fall on the boundaries, a relatively large amount of computation in the form of interpolation is required.

Numerical grid generation has been developed to tackle flow problems in irregular geometries. By this technique, a grid system is numerically generated from a set of partial differential equations. The grid nodes thus generated follow the shape of the flow configuration, and part of the new co-ordinate lines coincide with boundary segments of the physical plane. In essence, this technique maps an irregular shape in the physical domain into a rectangular shape in the computational domain, thus permitting the governing equations to be computed on a uniform mesh without the necessity for interpolation for the boundary points.

Applications of numerical grid generation and co-ordinate transformation to turbulent flow problems have recently appeared in the literature.[1–7] Although grid generation does help to simplify problems involving flow fields with arbitrarily shaped boundaries, it is obvious that as the geometry becomes more complex, grid generation itself also becomes a more difficult task. Construction of a single grid system that covers the entire flow field would be very difficult for complicated flows such as the flow through a gas turbine combustor with several passages. In such cases, a better approach would be to divide the field into several subregions and generate an

0271–2091/89/020167–17$08.50

Received 6 October 1987
Revised 10 May 1988

independent grid for each subregion. Grid generation would therefore be a much easier process. This method has been referred to as a zonal approach or a grid-patching technique. With the zonal approach, better utilization of the available number of grid points can be realized. Moreover, this approach facilitates the use of different computational methods in each of the zones. This has the potential to save computational time because less complicated schemes can be used in certain areas of the field. Moreover, a zonal approach provides a means for examining regions where results may be more sensitive to the numerical method employed.

The zonal grid method has been incorporated into many calculations involving solution of Euler's equation (e.g. References 8–12). However, it has not been applied to turbulent flows. Recently, Shyy[13] underscored the need for using zonal grid methods in turbulent flow computations. Shyy simulated turbulent flow in an annular dump diffuser. He found that a single grid system, generated over the whole domain, caused the grid density in the annular tube to be much larger than that in the dump region. Moreover, he experienced difficulty in refining the grid in sharp corner regions. This problem could be alleviated by using a zonal grid approach in which the dump diffuser is divided into two regions: a dump region with a fine mesh and an annular region with a coarse mesh.

The division of a given flow field into subregions introduces grid boundaries in the calculation domain. Since either grid lines or transformation metrics may not be continuous at the interface of any two zones, care must be exercised in treating interface points in order to transfer information accurately. In fact, proper zonal boundary treatment is a key ingredient for successful application of this technique.

The present study is aimed at the development of a zonal boundary scheme for the calculation of turbulent flow in complex geometries. The scheme will be tested for flow in a 45° expansion combustor and for flow in an axisymmetric annular bifurcated diffuser.

ANALYSIS

Governing equation and boundary conditions

The general form of the steady, time-averaged, equation governing axisymmetric turbulent flow may be written in general as

$$\frac{\partial}{\partial x}(\rho u\phi)+\frac{\partial}{r\partial r}(\rho vr\phi)-\frac{\partial}{\partial x}\left(\Gamma_\phi\frac{\partial\phi}{\partial x}\right)-\frac{\partial}{r\partial r}\left(r\Gamma_\phi\frac{\partial\phi}{\partial r}\right)=S_\phi, \tag{1}$$

where ϕ represents any of the dependent variables u, v, k and ε; S_ϕ is the source term for the variable ϕ which includes generation, dissipation and terms not covered by convection and diffusion; and Γ_ϕ is the effective exchange coefficient. Relations for Γ_ϕ and S_ϕ for each variable and the constants appearing in the turbulence model can be found elsewhere (e.g. References 14 and 15). Since the flow domains are assumed to be irregular, the governing equations will be expressed in a non-orthogonal curvilinear co-ordinate system. The chain rule is used to introduce new independent variables ξ and η which replace x and r in equation (1). The transformed equations are

$$\frac{\partial}{J\partial\xi}(\rho F_\xi\phi)-\frac{\partial}{J\partial\xi}\left[\frac{\Gamma_\phi}{J}\left(\alpha\frac{\partial\phi}{\partial\xi}-\beta\frac{\partial\phi}{\partial\eta}\right)\right]+\frac{\partial}{rJ\partial\eta}(\rho rF_\eta\phi)-\frac{\partial}{rJ\partial\eta}\left[\frac{\Gamma_\phi r}{J}\left(\gamma\frac{\partial\phi}{\partial\eta}-\beta\frac{\partial\phi}{\partial\xi}\right)\right]$$
$$=S_\phi(\xi,\eta), \tag{2}$$

where

$$F_\xi=ur_\eta-vx_\eta, \qquad F_\eta=vx_\xi-ur_\xi$$

and the geometric factors α, β, γ and J are defined as

$$\alpha = x_\eta^2 + r_\eta^2, \qquad \beta = x_\xi x_\eta + r_\xi r_\eta, \qquad \gamma = x_\xi^2 + r_\xi^2, \qquad J = x_\xi r_\eta - x_\eta r_\xi.$$

The physical significance of several of the terms given above may be advanced: $F_\xi/\sqrt{\alpha}$ and $F_\eta/\sqrt{\gamma}$ are the covariant velocity components normal to lines of constant η and ξ respectively; $\sqrt{\alpha}$ and $\sqrt{\gamma}$ represent the distances between two grid points in the η and α directions; β is the measure of the orthogonality between the ξ and η lines—β vanishes when these co-ordinate lines are orthogonal; finally, J denotes a differential area element in the (ξ, η) plane.

Equation (2) has been used by Shyy[13] to solve for turbulent flow in a dump diffuser. A plane two-dimensional form of this equation was used by Rhie and Chow[6] to determine flow past an isolated aerofoil. Further, a three-dimensional form was used by Hah[7] for flow in a turbine blade row.

Boundary conditions for the above equation in the transformed domain are derived from physical arguments. At the inlet, Dirichlet conditions are applied and the dependent variables in both co-ordinates remain the same, so that

$$\phi(\xi, \eta) = \phi(x, r). \tag{3}$$

At the flow outlet and along the duct centreline, Neumann boundary conditions are generally employed. The derivatives of a variable in a direction normal to a constant-ξ line and a constant-η line are given respectively as

$$\left.\frac{\partial \phi}{\partial n}\right|_\xi = \frac{1}{J\sqrt{\alpha}}\left(\alpha \frac{\partial \phi}{\partial \xi} - \beta \frac{\partial \phi}{\partial \eta}\right), \qquad \left.\frac{\partial \phi}{\partial n}\right|_\eta = \frac{1}{J\sqrt{\gamma}}\left(\gamma \frac{\partial \phi}{\partial \eta} - \beta \frac{\partial \phi}{\partial \xi}\right). \tag{4}$$

At the solid boundaries, a wall function is used to provide the boundary conditions for nodes nearest the surface.[14]

Solution method

Equation (2) is solved in the transformed co-ordinate system by employing the finite volume method to discretize the equation and by incorporating the SIMPLE algorithm.[16] The SIMPLE algorithm involves a series of steps of prediction and correction for the coupling of velocities and pressure.

The finite difference equation for the prediction of velocities is obtained by integrating the governing equation over a control volume in a staggered grid system and using appropriate finite differencing methods to represent the convective and diffusion terms at the control volume boundaries. In present study, three differencing methods—hybrid, quadratic upwind[17] and skew upwind[18]—were used for the convective flux, and central differencing was used for the diffusion flux. Upon introduction of these forms of differences, a discretized relation between the variable at a central point P and its neighbouring values is obtained, namely

$$A_P \phi_P = A_E \phi_E + A_W \phi_W + A_N \phi_N + A_S \phi_S + S_\phi J r - \frac{\Gamma_\phi}{J} r_\beta \left.\frac{\partial \phi}{\partial \eta}\right|_w^e - \frac{\Gamma_\phi}{J} r_\beta \left.\frac{\partial \phi}{\partial \xi}\right|_s^n. \tag{5}$$

In this expression the A are the coefficients of the convective and diffusion fluxes obtained for the various differencing schemes. The terms containing β are usually small and are combined with the source term, and treated as known quantities using the most recently available values. It is noted that both quadratic and skew methods involve nine points in the interpolation of the convective flux. In order to fit a five-point stencil, the extra terms in these methods are lumped into the source terms. Because equation (5) has the same form as derived from a Cartersian co-ordinate system, the SIMPLE algorithm as originally presented can be used without alteration. The

matrix is solved using the tridiagonal matrix algorithm (TDMA) and by a line-by-line iteration method; line sweeps are in the primary flow direction, so that the change of flow condition from upstream can be immediately conveyed downstream. The velocity field obtained from equation (5), however, may not satisfy the continuity equation and requires adjustment. The adjustment of velocities is connected to the pressure change, denoted here as p', through the following formulae:

$$u = u^* + D^u\left(-r_\eta \frac{\partial p'}{\partial \xi} + r_\xi \frac{\partial p'}{\partial \eta}\right), \qquad v = v^* + D^v\left(-x_\xi \frac{\partial p'}{\partial \eta} + x_\eta \frac{\partial p'}{\partial \xi}\right). \tag{6}$$

These equations can be derived from the corresponding momentum equations. Substituting the corrected velocities into the continuity equation and integrating over a control volume yields a partial differential equation governing the pressure correction p':

$$\dot{m}_p = \left(-\rho r \alpha' \frac{\partial p'}{\partial \xi} + \rho r \beta' \frac{\partial p'}{\partial \eta}\right)\Bigg|_w^e + \left(-\rho r \gamma' \frac{\partial p'}{\partial \eta} + \rho r \beta' \frac{\partial p'}{\partial \xi}\right)\Bigg|_s^n, \tag{7}$$

where

$$\alpha' = D^v x_\eta^2 + D^u r_\eta^2, \qquad \beta' = D^v x_\xi x_\eta + D^u r_\xi r_\eta, \qquad \gamma' = D^v x_\xi^2 + D^u r_\xi^2$$

and $\dot{m}_p$ is the continuity equation imbalance based on predicted velocites. Since the cross-derivative β' terms are relatively small, it was found that solutions obtained by omitting them were not greatly affected. Therefore these terms were dropped and a central difference was used for the derivatives of p'. The final form of equation (7), written in an analogous fashion to equation (5), is then

$$A_P p'_P = A_E p'_E + A_W p'_W + A_N p'_N + A_S p'_S + \dot{m}_p. \tag{8}$$

The boundary conditions for the p' equation are that the derivatives in the normal direction on the boundaries vanish. Values of the pressure on the boundary were linearly extrapolated from the values at the interior points.

Once the velocities were predicted and corrected, F_ξ and F_η were then calculated to update the mass flow rate. The mass flow rate through each axial plane was monitored after each iteration, and when the residue divided by the inlet mass flow rate was less than 10^{-4}, the solution was regarded as converged.

Zonal boundary scheme

In the use of a zonal grid approach, the mesh for various regions of the field is generated separately. Therefore the grid lines extending across two adjoining regions may not align with each other, and the transformation metrics across the zonal interface may not be continuous. Computation using a zonal grid method is based on the idea that each region of the field may be treated independently as a boundary value problem. The required boundary conditions were obtained either from physical arguments or from information supplied from adjacent regions using proper zonal boundary schemes. Across zone interfaces, two considerations must be observed: continuity of the dependent variables and conservation of fluxes. In the present work a conservation form is developed that uses an interpolation method to transfer data from a coarse grid region to a fine grid region, and an integration method is used for the reverse process.

Consider the pair of discontinuous grids shown in Figure 1; the fine grid region is called zone 1 and the coarse grid region zone 2. Suppose the solution is to be advanced on the fine grid zone. The calculation of the dependent variables at the position of line AB requires values at the downstream points. To obtain the values at these points from zone 2, an overlapping region is generated by extending the constant-η^f lines of zone 1 into zone 2 to intersect with the line CD.

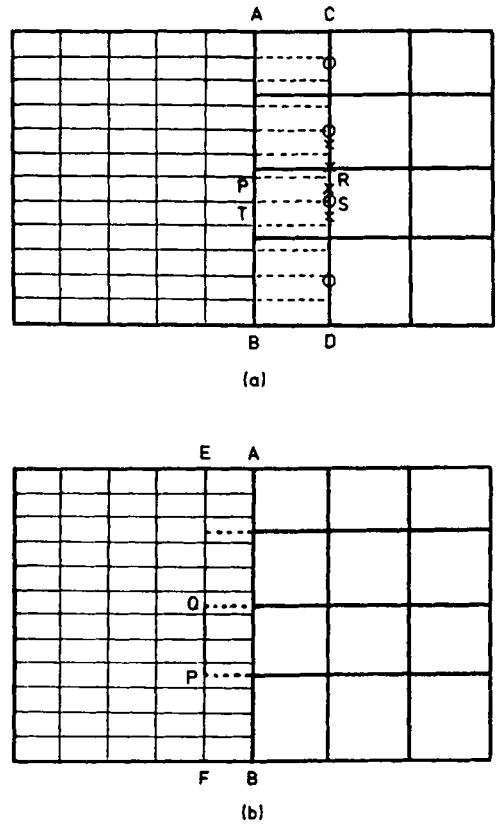

Figure 1. Zonal boundary scheme for (a) updating fine grid points, (b) updating coarse grid points

This overlapping forms extra control volumes at the outlet of zone 1. Values of the dependent variables enclosed in these outer control volumes located either at the cell face or at its centre are obtained by interpolation of values from the coarse grid. For example, a variable located at the cell face (marked $\times$) of a control volume PRST in Figure 1(a) is found by the interpolation of values from its coarse grid neighbouring points (marked $\bigcirc$). The values at the $\times$ locations are then adjusted in order to satisfy global conservation as calculated from the coarse grid at the same cross-section. The global conservation property is satisfied by requiring that

$$\int_D^C g^f \mathrm{d}\eta^f = \int_D^C g^c \mathrm{d}\eta^c, \tag{9}$$

where g^f and g^c are the fluxes through the zonal boundary CD for zone 1 and zone 2 respectively, and $\mathrm{d}\eta^f$ and $\mathrm{d}\eta^c$ are the corresponding elements of area normal to the flow direction. In a similar manner, flow properties located at the cell centre can also be updated. The accuracy of the results depends upon the order of the interpolation scheme. A third-order Lagrange polynomial was used to interpolate the values of u, v and p. However, a higher-order polynomial might over- or under-correct the interpolated values. When this method was applied to interpolate turbulence quantities, owing to the large variation in the radial direction, unrealistic negative kinetic energy or dissipation energy values were obtained. Therefore a linear scheme was used.

To update the zonal boundary points of the coarse grid, the overlapped region is constructed by extending the constant-η^f lines of zone 2 into zone 1. Consequently, these lines will intercept the line EF and form control volumes outside zone 2. The dependent variables enclosed in these exterior control volumes are established by an integration method which preserves the conservation properties of flow across the cell boundaries. For a control volume in the coarse grid having the boundary PQ, as shown in Figure 1(b), the flux across this area must equal that crossing the corresponding boundaries of the fine grid, i.e.

$$g^c = \frac{1}{\Delta\eta^c} \int_P^Q g^f d\eta^f. \tag{10}$$

If a piecewise constant variation of g between two grid points is assumed, the above equation can be rewritten in discretized form as

$$g^c = \frac{1}{\Delta\eta^c} \sum_{j=P}^{Q} g_j^f \Delta\eta_j^f N_j, \tag{11}$$

where N_j is the fraction of flux of each control volume in zone 1 that enters the corresponding control volume of zone 2. It is noted that when $\Delta\eta^c$ equals $\Delta\eta^f$, g^c will be equal to g^f and the flow properties will vary continuously across the boundary.

The zonal boundary procedure was applied at each iteration. When the computation was advanced from one zone to another, the zonal boundary points were first updated and then the interior points were computed.

RESULTS AND DISCUSSION

To verify the numerical methods developed above, predicted results are compared with existing experimental values for flow in a 45° expansion combustor and in a annular bifurcated diffuser.

Flow in a 45° expansion combustor

To simulate this flow, the inlet boundary conditions were taken from experimental conditions obtained by Chaturvedi:[19] the velocity profile was flat and the Reynolds number was $2{\cdot}5 \times 10^5$. The duct expansion ratio is 2·0. The inlet conditions for turbulence kinetic energy and dissipation energy were not provided by Chaturvedi and therefore had to be estimated. According to Gosman *et al.*[20] and Lilley and Rhode,[15] the latter two parameters may be written as $k = 0{\cdot}03u_{in}^2$ and $\varepsilon = k^{1{\cdot}5}/0{\cdot}005D$.

The flow domain of a 45° expansion combustor is divided into two zones separated by a zonal boundary. A fine grid was used to cover the inlet zone and the recirculation region, and a coarse

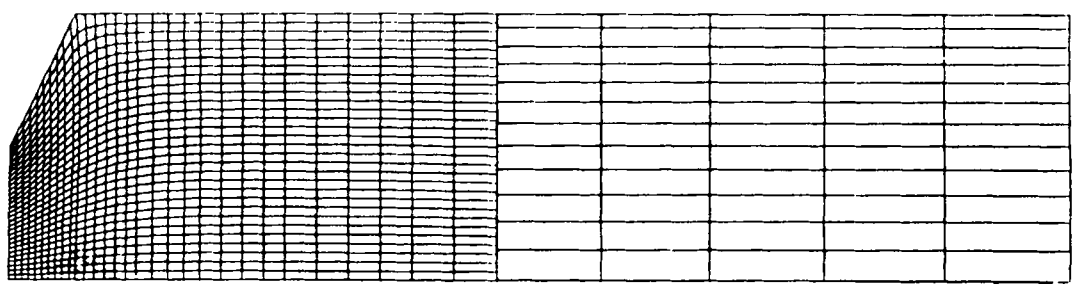

Figure 2. Grid distribution for a 45° expansion combustor

grid was used to cover the downstream region. In the fine grid zone, two nets were used: 30×30 and 15×20. In the coarse grid zone, only a 5×12 net was constructed. The grid lines were evenly spaced in the radial direction but clustered in the flow inlet. Figure 2 shows the grid distribution for a 30×30 fine grid and the 5×12 coarse mesh. The discontinuity of co-ordinate lines at the zone interface is self-evident. Prior to the grid selection, calculations using a single grid system were made on a 41×22 and on a 46×29 mesh. The grid lines were clustered at the flow inlet and near the solid wall. The reattachment lengths predicted from both grid systems were found to be comparable. Therefore it is not expected that the results can be significantly improved by increasing the number of grid points. Consequently, the number of grid nodes used in the zonal grid approach is chosen to be the same as that used for the single grid system. Prior testing with different computational schemes revealed that the final solution was determined more by how the flow was calculated in the upstream region than by what differencing methods were used in the downstream zone. From this observation, and the fact that the downstream flow is nearly parallel to the axial co-ordinate lines, thus minimizing the diffusion error due to flow direction and grid line skewness, computations were made using various differencing schemes in the fine grid zone, while the hybrid scheme was always applied in the coarse grid region.

The reattachment length of the recirculation was first examined. Table I presents the calculated results for various computational schemes and meshes. Also listed is the measured length as reported by Chaturvedi.[19] This value is 4·5 times the inlet diameter. The differences between the predicted and measured lengths range from 10 to 30% depending upon the numerical methods considered. The hybrid scheme produced the most accurate results of the three differencing schemes tested. Predictions based on the quadratic upwind scheme are mixed, while those based on the skew upwind scheme are seen to be very low for both the single and the zonal grid calculations. There are several possible sources for the discrepancies, which include the turbulence model, the numerical method and the grid system. At this point, it is not known which of these factors contributes the most to the discrepancy.

The velocity profiles computed on the 30×30–5×12 zone mesh system are shown in Figure 3. The results from the other two grid systems are similar and therefore are shown here. The predictions compare favourably with the experimental data for most locations. The poorest agreement occurs in the middle portion of the duct at $x/D = 3{\cdot}0$. In the wall region, the predicted velocities vary according to the differencing method used. Consequently, estimation of the reattachment length can be expected to differ even though the velocity field comparison is good for most regions of the flow. The velocity decay along the duct centreline is shown in Figure 4. The comparison is seen to be reasonably good within the recirculation region, but produces overestimated results farther downstream for the three differencing methods used. The radial distributions of turbulence intensity at different stations are shown in Figure 5. Since $\overline{u'u'}$ was

Table I. Reattachment length of a 45° expansion combustor

Measurement: 4·5			
Prediction			
	41×22	$15 \times 20, 5 \times 12$	$30 \times 30, 5 \times 12$
Hybrid	4·19	3·88	4·14
Quadratic	4·05	4·84	3·95
Skew	3·04	3·15	3·35

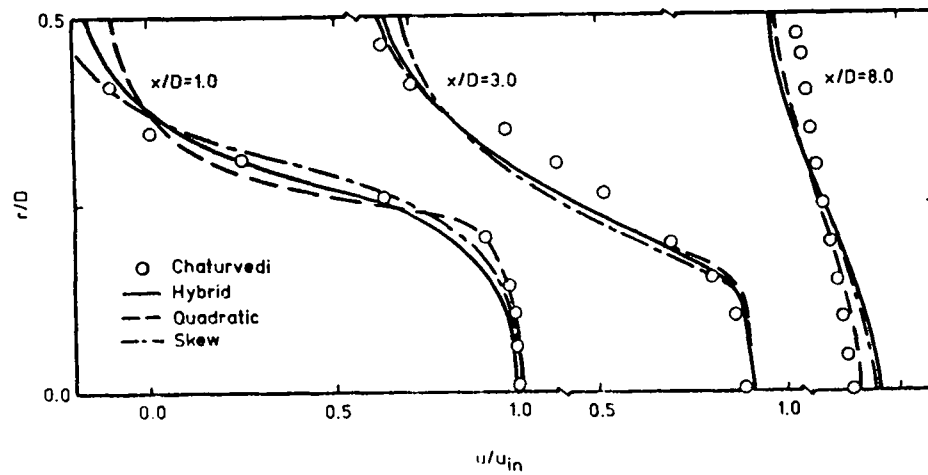

Figure 3. Axial velocity profiles at various locations for flow in a 45° expansion combustor

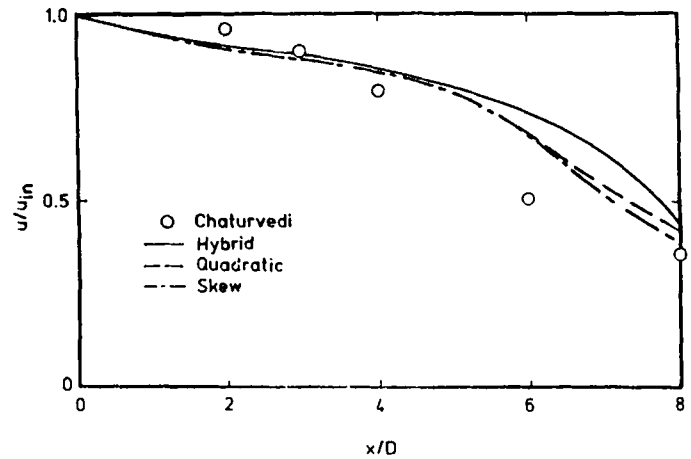

Figure 4. Centreline velocity for flow in a 45° expansion combustor

measured in the experiments, in order to make the comparison, it was assumed that the velocity fluctuations were the same in all directions, so $u' = \sqrt{(2k/3)}$. The predictions were not accurate at the upstream positions shown, i.e. at $x/D = 1{\cdot}0$ and $3{\cdot}0$. On the other hand, the predictions were in good agreement with the experimental values at the position $x/D = 8{\cdot}0$. The maximum error occurred at $r/D = 0{\cdot}5$ and was approximately 15%. At $x/D = 1{\cdot}0$ and $3{\cdot}0$ the calculated values are, for the most part, well below the measured values. The error, as pointed out by Habib and Whitelaw,[3,21] arises from the extra strain terms in the calculation of both the Reynolds stresses and the dissipation rate, and from inappropriate application of Boussinesq's hypotheses.

Figures 6–8 depict streamline contours of the flow, and contours of the axial velocity and the turbulence intensity respectively. These plots are based on the calculations using the hybrid scheme. The contours in each zone are plotted independently of each other. Lines of constant

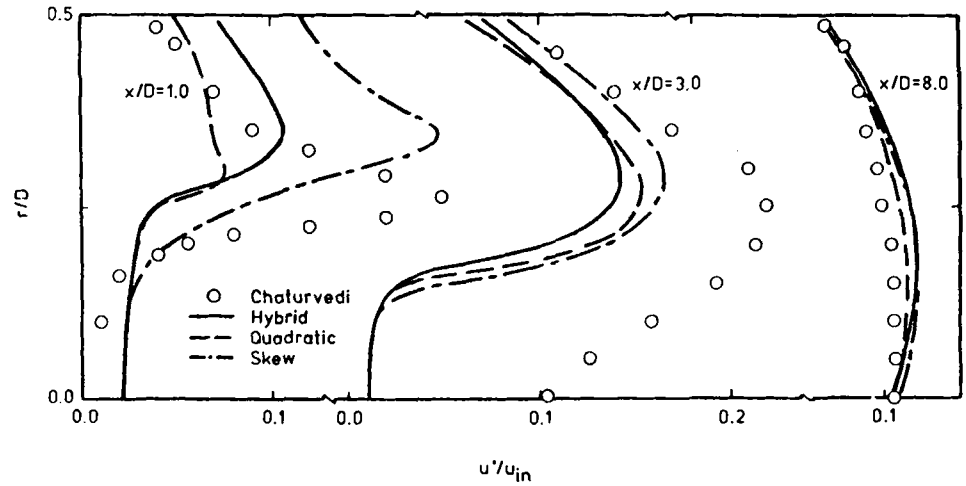

Figure 5. Turbulence intensity at various axial locations for flow in a 45° expansion combustor

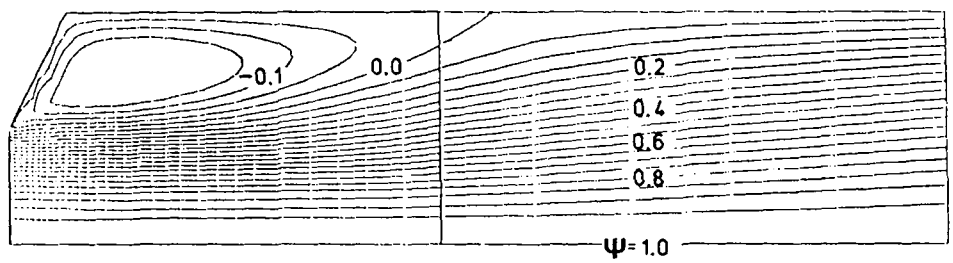

Figure 6. Streamlines of the flow in a 45° expansion combustor

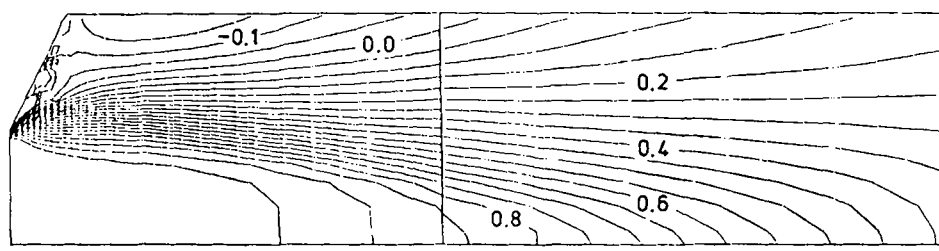

Figure 7. Axial velocity contours for flow in a 45° expansion combustor

velocity and the flow streamlines are seen to be continuous across the zonal boundary. However, discontinuities in the contours of the turbulence intensity may be observed because a less accurate interpolation scheme was used for this variable. These plots are similar to the predictions of Habib and Whitelaw[3] and are also compatible with Chaturvedi's measurements.[19] The maximum reverse flow was found to be about 18% of the total mass flow rate at a location approximately one inlet diameter downstream of the flow inlet. High turbulence intensity was generated along the shear layer, and the maximum value was located at the position $x/D = 3{\cdot}0$.

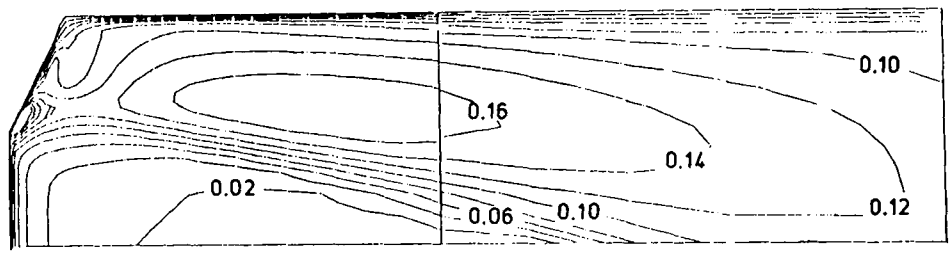

Figure 8. Turbulence intensity contours for flow in a 45° expansion combustor

Flow in an annular bifurcated diffuser

The annular bifurcated combustor prediffuser is designed to provide maximum efficiency, in terms of the pressure recovery, for the shortest length. The diffuser divides the flow into two parallel passages and directs almost equal amounts of flow to corresponding combustor chambers.

The flow simulation uses the experimental conditions of Lown *et al.*[22] In their experiments, three different inlet velocity profiles were generated to test the performance of the diffuser, but only one of them, designated as the centre peaked velocity profile, is employed in this study. At the inlet, the Reynolds number is approximately $2{\cdot}2 \times 10^5$ and the Mach number is about 0·247. Thus the fluid can be treated as incompressible. The inlet conditions of kinetic energy and dissipation rate were estimated as in the 45° expansion combustor case. Since the diffuser is short, the usual boundary condition of zero normal gradient for dependent variables at the exit may not be realized. Thus the exit boundary condition is assumed to be such that the second derivative of each variable with respect to ξ is zero. The velocity components at the outlet of both ducts are obtained from inner values and adjusted to satisfy the overall mass conservation. It is noted that flow rates through the inner duct and the outer duct were not specified, but rather were permitted to seek individual balances. The bifurcated diffuser was divided into three computational zones: an inlet zone, and upper and lower branch zones. Two different grid systems were used in the computations. The coarse grid has an 11×15 mesh in the inlet area and a 14×11 mesh in each of the upper and lower branches. The fine grid has 16×25, 21×17 and 21×17 grid points for the inlet and the two branches respectively. The grid distribution for the zoned grid system is shown in Figure 9. Because each flow region is enclosed by a simple block, the grids were easier to generate.

The ratio of the mass division for various differencing methods and grid systems was examined and is tabulated in Table II. The table also includes the measured values and the results computed from a 36×25 single grid mesh. The skew upwind difference scheme and the hybrid difference scheme produced results with less grid dependency, and differed by approximately 3·5% from the measured values. On the other hand, the predictions based on the quadratic difference scheme did not possess these characteristics; the results were found to be better when using the coarse grid than when using the fine grid. On the fine grid, the mass flow rate was overpredicted in the outer duct and underpredicted in the inner duct. The velocity distributions at the diffuser outlet are compared with experiments in Figure 10. The experimental data were scaled so as to have the same basis as that used in the simulation. It can be seen that the predicted shapes of the velocity profiles generally agree with the experimental data. However, there is a difference between predicted and measured values in the regions near the solid wall. The velocity contours obtained by using the three differencing methods are shown in Figure 11. The distributions are similar for

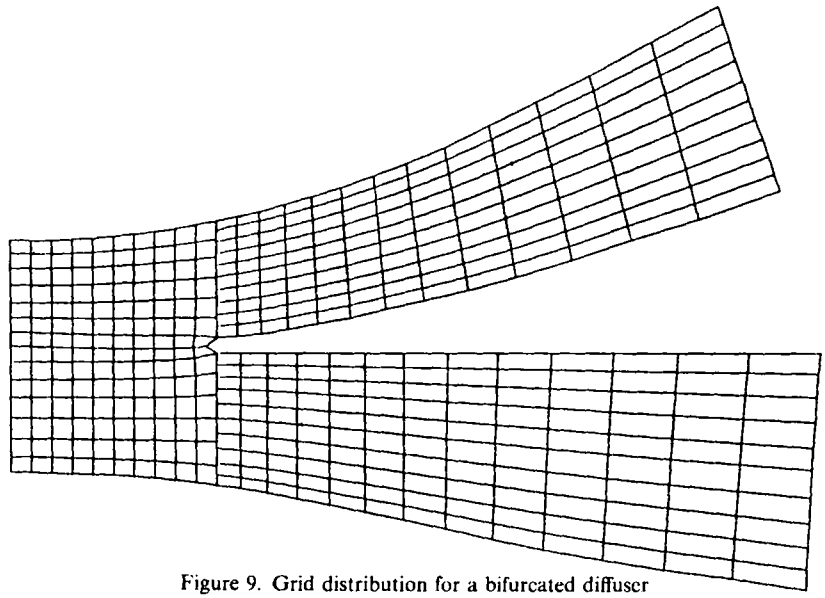

Figure 9. Grid distribution for a bifurcated diffuser

Table II. Mass split ratio in a bifurcated diffuser

Measurement: outer duct 48%, inner duct 52%

Prediction

	31 × 25		11 × 15, 14 × 11, 14 × 11		16 × 25, 21 × 17, 21 × 17	
	Outer	Inner	Outer	Inner	Outer	Inner
Hybrid	49·4	50·6	48·1	51·9	46·3	53·7
Quadratic	49·0	51·0	46·8	53·2	51·2	48·8
Skew	49·2	50·8	47·2	52·8	48·6	51·4

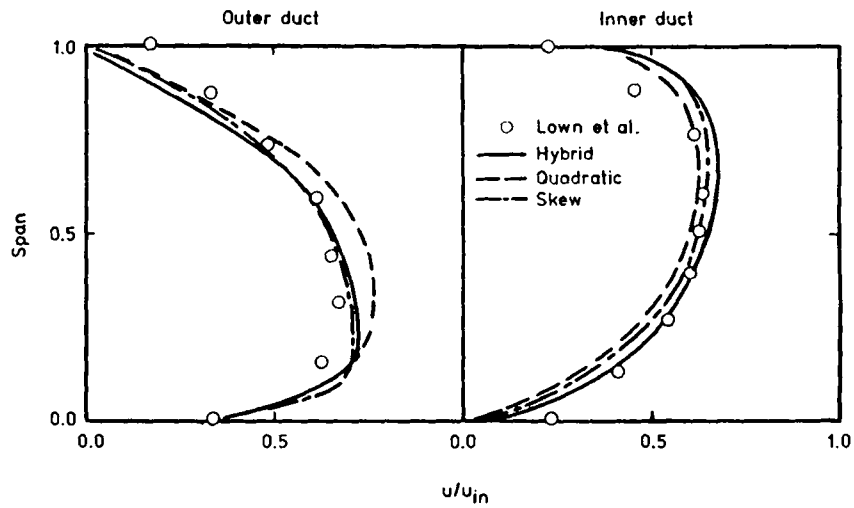

Figure 10. Velocity profiles at the outlet of a bifurcated diffuser, computed on a fine zoned grid

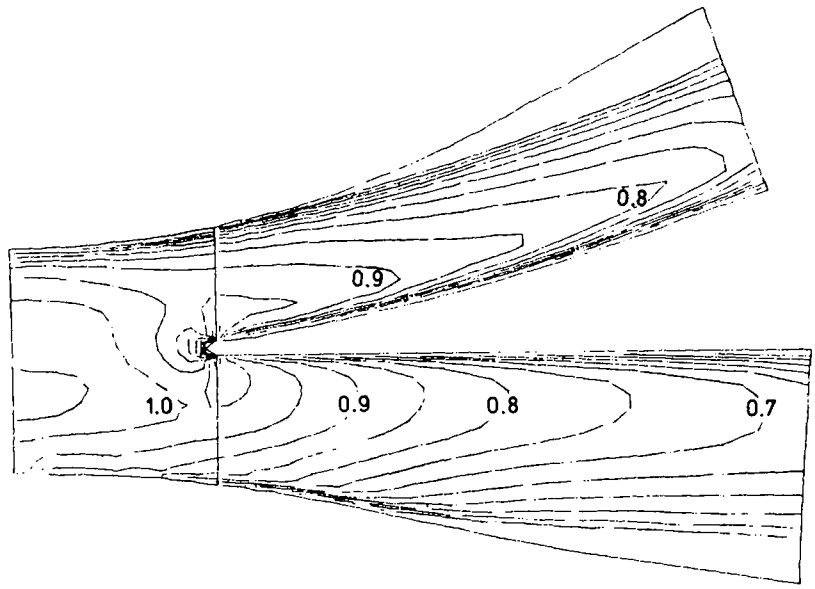

(a)

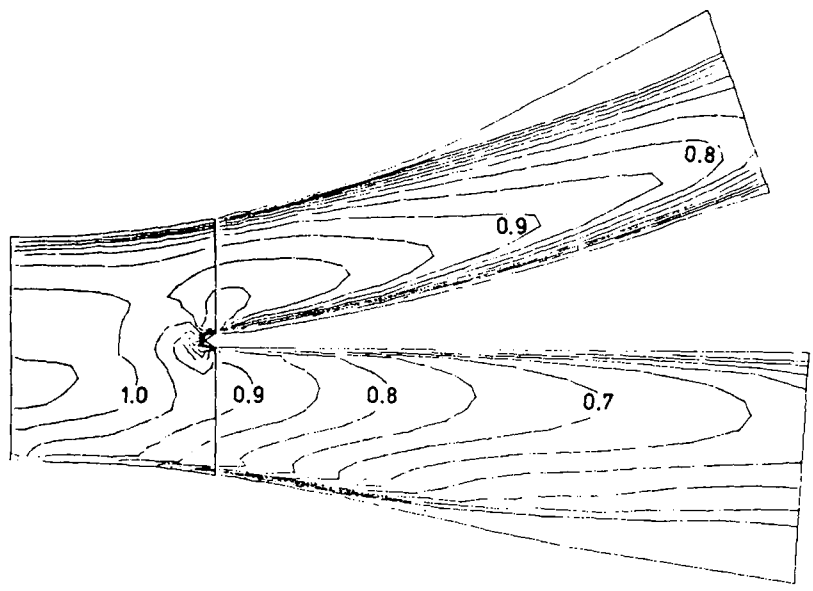

(b)

Fig. 11 (a–b)

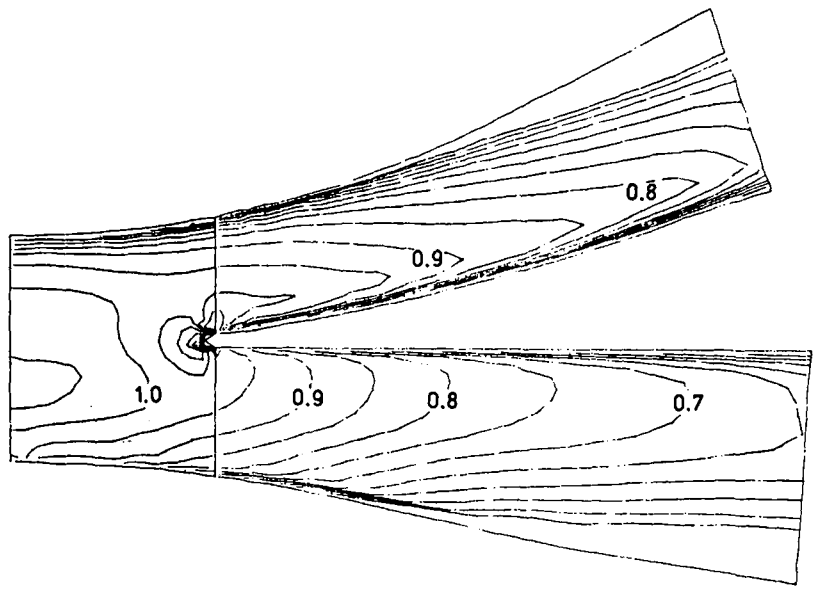

Figure 11. Velocity contours for flow in a bifurcated diffuser: (a) hybrid; (b) quadratic; (c) skew

the hybrid and the skew upwind scheme, but show some differences at the upper duct for the quadratic upwind scheme because of the overprediction of the velocity by this scheme. Across the zonal boundaries, the contours are observed to be smooth at most locations. Near the upper wall, some discontinuity occurs. In that region, the velocity gradient is large; consequently it is felt either the interpolation scheme or the plotting routine could cause this discontinuity. Lines of constant pressure coefficient are shown in Figure 12. A discontinuity is observed at the position where the ducts divide. The pressure is very high at the apex of the flow divider and abruptly decreases along the divider wall; the pressure gradients are so large that, in addition to the reason mentioned above, the grid in this region may not be fine enough to completely describe the pressure distribution. At the exit of the outer duct, the predicted results are somewhat different depending on the numerical method used. All three methods predicted separation at the upper corner. However, this flow separation phenomenon was not observed in the experiments. The pressure coefficients along the inner and outer casings are compared in Figures 13(a) and 13(b) respectively. The predicted results shown in Figure 13 are the average values of those obtained by the three differencing methods. Along the outer wall the prediction is reasonably good, although the error is large—nearly 30% at some locations. On the inner wall the methods used overestimate the pressure. It is not clear whether the disagreement is related to the computations or attributable to some experimental difficulty.

In both the 45° combustor geometry and the bifurcated diffuser, it is found that predictions using the quadratic or the skew upwind schemes are not better than that based on the hybrid scheme. The purpose of incorporating advanced differencing schemes is to reduce the false diffusion which occurs when the flow is oblique to the grid lines. However, in this study, the stream-to-grid angle is small except in the recirculation region; false diffusion does not appear to

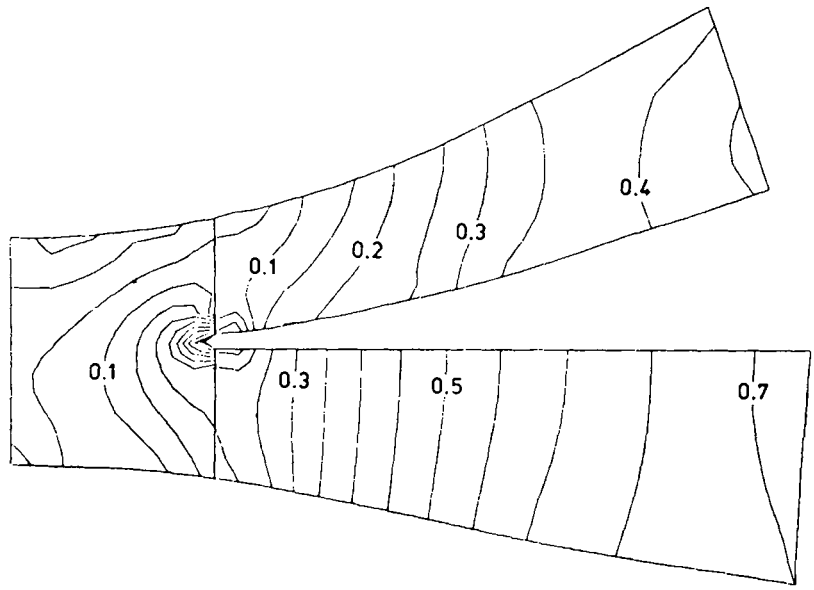

(a)

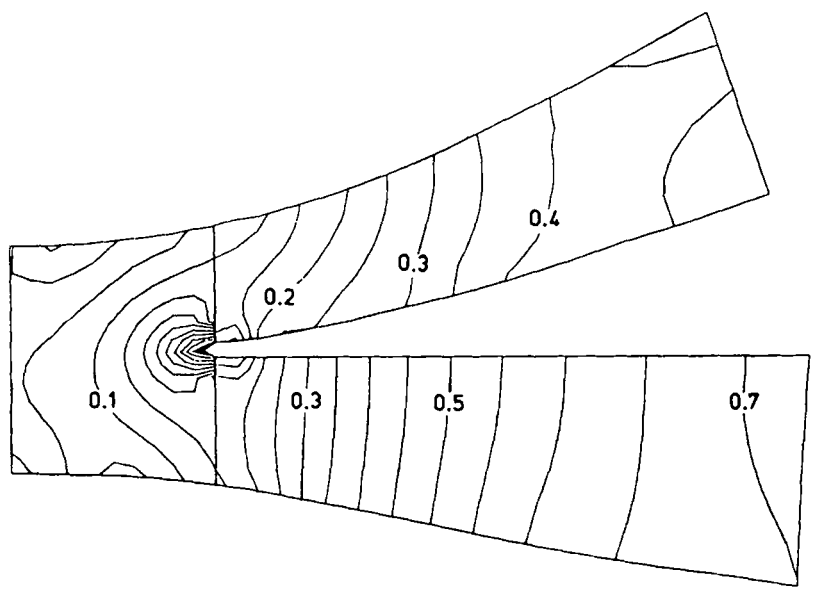

(b)

Fig. 12 (a–b)

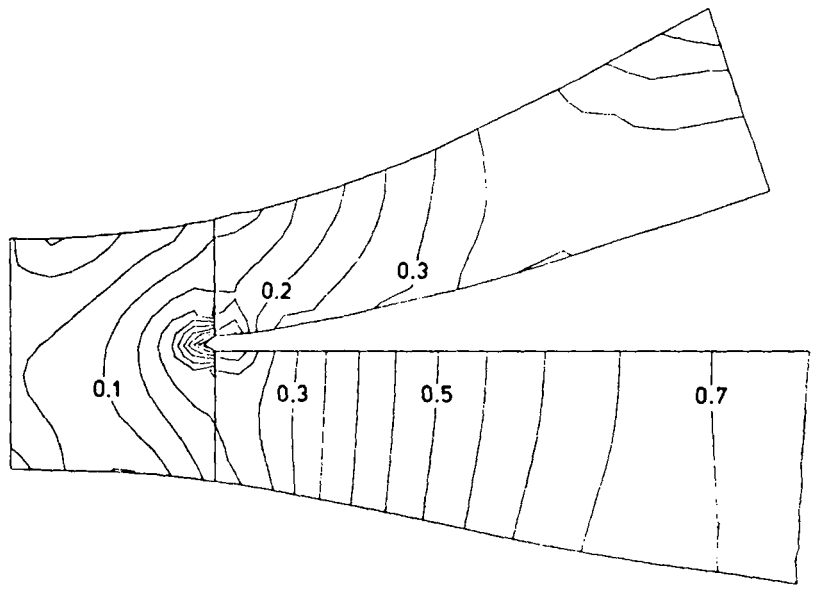

(c)

Figure 12. Pressure distribution in a bifurcated diffuser: (a) hybrid; (b) quadratic; (c) skew

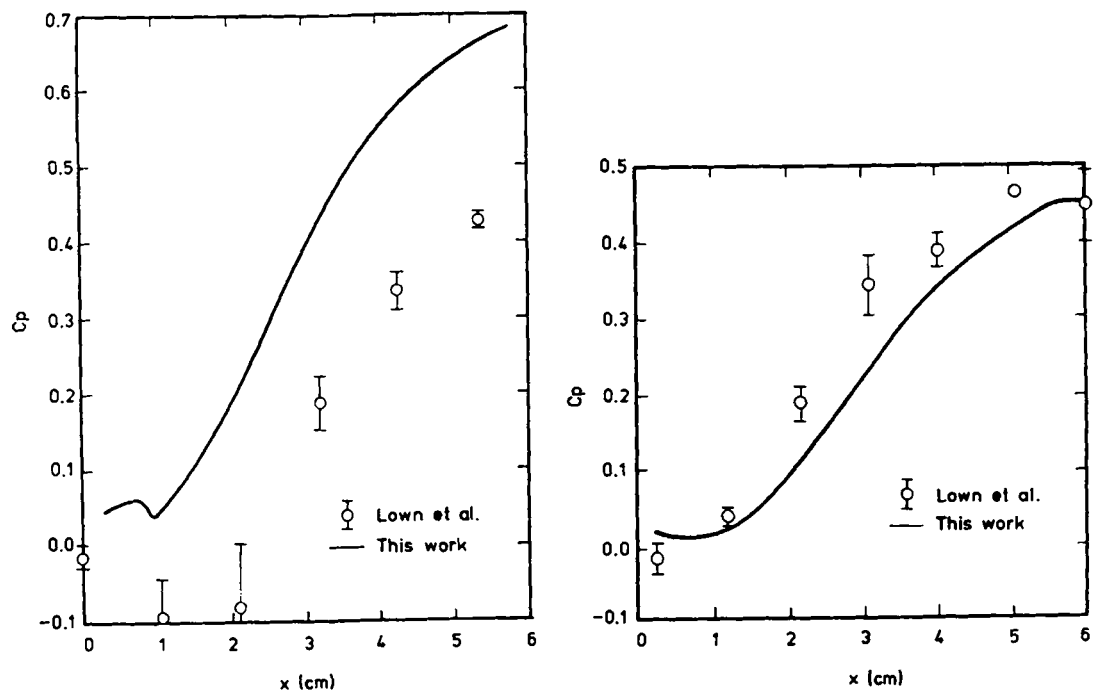

(a) (b)

Figure 13. Pressure coefficient along the casing of a bifurcated diffuser: (a) inner casing; (b) outer casing

be a problem. In addition to the low oblique angles, the effective viscosity in turbulence flow is much larger than the molecular viscosity, hence false diffusion becomes less important.[23]

CONCLUDING REMARKS

Turbulent flows in different combustor and diffuser geometries were predicted using a body-fitted co-ordinate transformation and a zonal grid method. By the latter, the entire flow field was partitioned into subsections each having its own grid density and local computational scheme. A conservative scheme was developed to generate the zonal boundary conditions. The zonal boundary scheme was numerically stable in the test cases and permitted flow properties to be transferred smoothly across the interface. From the foregoing computations, it has been demonstrated that zonal grid calculations are capable of producing results that are in reasonable agreement with measured values and are of the same quality as those using a single grid system. The zonal approach has the additional advantage of permitting optimized utilization of the overall grid points for the best resolution. Unfortunately, the computation, when crossing a zone interface, requires either integration or interpolation to update the boundary points of another zone. This additional procedure requires extra computer time, which tends to offset the savings from using less grid points.

Quadratic upwind and skew upwind differencing methods have been incorporated into the solution algorithm to evaluate the influence of numerical diffusion. From comparisons of the velocity, pressure and turbulence intensity distributions, it is seen that these advanced schemes did not show any significant improvement over conventional hybrid differencing.

ACKNOWLEDGEMENTS

The work reported in this paper was supported by a grant through the Combustion Group at NASA Lewis Research Center, Cleveland, Ohio. The authors wish to express their gratitude to Russ Claus, the grant monitor, for his support and encouragement throughout the term of this research.

REFERENCES

1. S. B. Pope, 'The calculation of turbulent recirculating flows in general orthogonal coordinates', *J. Comput. Phys.*, **26**, 197 (1978).
2. I. Demirdzic, A. D. Gosman and R. I. Issa, 'A finite volume method for the prediction of turbulent flow in arbitrary geometries', in W. C. Reynolds and R. W. MacCormack (eds), *Lecture Series in Physics, Vol. 141*, Springer-Verlag, Berlin, 1981.
3. M. A. Habib and H. Whitelaw, 'The calculation of turbulent flow in wide-angle diffusers', *Numer. Heat Transfer*, **5**, 145 (1982).
4. F. Pourahmadi and J. A. C. Humphrey, 'Prediction of curved channel flow with an extended k–e model of turbulence', *AIAA J.*, **21**, 1365 (1983).
5. W. Shyy, S. M. Correa and S. S. Tong, 'Demonstration of a new body-fitted coordinate code for modeling gas turbine combustor flows', *AIAA 84-1381*, Cincinnati, Ohio, 1984.
6. C. M. Rhie and W. C. Chow, 'Numerical study of the turbulent flow past an airfoil with trailing edge separation', *AIAA J.*, **21**, 1525 (1983).
7. C. Hah, 'A Navier–Stokes analysis of three-dimensional turbulent flows inside turbine blade rows at design and off-design conditions', *AIAA Paper 83-GT-40*, 1983.
8. K. A. Hessenius and T. H. Pulliam, 'A zonal approach to solution of the Euler equation', *AIAA 82-0969*, St. Louis, MO, 1982.
9. M. M. Rai, 'A conservative treatment of zonal boundaries for Euler equation calculation', *AIAA 84-0164*, 1984.
10. M. M. Rai and K. A. Hessenius, 'Metric-discontinuous zonal grid calculation using the Osher scheme', *Comput. Fluids*, **12**, 161 (1984).

11. H. Atta Essam and J. Vadyak, 'A grid overlapping scheme for flowfield computations about multicomponent configurations', *AIAA J.*, **21,** 1271 (1983).
12. C. L. Reed and S. L. Karman, 'Multiple-block grid method applied to complex 3-D geometries', *SIAM 1986 National Meeting*, Boston, MA, July 1986.
13. W. Shyy, 'A further assessment of numerical annular dump diffuser flow calculations', *AIAA 85-1440*, Montery, California, 1985.
14. B. E. Launder and D. B. Spalding, 'The numerical computations of turbulent flows', *Comput. Methods Appl. Mech. Eng.*, **3,** 269 (1974).
15. D. G. Lilley and D. L. Rhode, 'A computer code for swirling turbulent combustor geometries', *NASA Contractor Report 3442*, 1982.
16. S. V. Patankar, *Numerical Heat Transfer and Fluid Flow*, Hemisphere Publishing Corporation, New York, 1980.
17. B. P. Leonard, 'A stable and accurate convective modelling procedure based on quadratic upstream interpolation', *Comput. Methods Appl. Mech. Eng.*, **19,** 59 (1979).
18. G. D. Raithby, 'Skew upstream differencing schemes for problems involving fluid flow', *Comput. Methods Appl. Mech. Eng.*, **9,** 153 (1976).
19. M. C. Chaturvedi, 'Flow characteristics of axisymmetric expansions', *J. Hydraul. Div. Proc. ASCE*, **89,** 61 (May, 1963).
20. A. D. Gosman, E. E. Khalil and J. H. Whitelaw, 'The calculation of two dimensional turbulent recirculating flows', *Turbulent Shear Flows*, Vol. *1*, Springer-Verlag, 1979.
21. M. A. Habib and H. Whitelaw, 'Velocity characteristics of confined coaxial jets with and without swirl', *J. Fluid Eng.*, **102,** 47 (1980).
22. H. Lown, P. A. Sabla and J. R. Taylor, 'Energy efficient engine component development and integration— combustor inlet diffuser aerodynamics performance evaluation', *R80AEG611*, General Electric, 1980.
23. E. E. Khalil, *Modeling of Furnaces and Combustors*, Abacus Press, 1982.